Thermodynamic and electron transport properties of $Ca_3Ru_2O_7$ from first-principles phonon calculations and Boltzmann transport theory

Yi Wang [1,*] Yihuang Xiong [1,†] Tiannan Yang,[1] Yakun Yuan [2] Shun-Li Shang [1] Zi-Kui Liu [1] Venkatraman Gopalan,[1] Ismaila Dabo,[1] and Long-Qing Chen[1]

[1]*Department of Materials Science and Engineering, The Pennsylvania State University, University Park, Pennsylvania 16802, USA*

[2]*School of Department of Mechanical Engineering and Zhangjiang Institute for Advanced Study, Shanghai Jiao Tong University, Shanghai 200240, China*

(Received 8 August 2022; accepted 14 December 2022; published 11 January 2023)

This work demonstrates a first-principles-based approach to obtaining finite temperature thermal and electronic transport properties which can be employed to model and understand mesoscale structural evolution during electronic, magnetic, and structural phase transitions. A computationally tractable model was introduced to estimate electron relaxation time and its temperature dependence. The model is applied to $Ca_3Ru_2O_7$ with a focus on understanding its electrical resistivity across the electronic phase transition at 48 K. A quasiharmonic phonon approach to the lattice vibrations was employed to account for thermal expansion while the Boltzmann transport theory including spin-orbit coupling was used to calculate the electron-transport properties, including the temperature dependence of electrical conductivity.

DOI: 10.1103/PhysRevB.107.035118

I. INTRODUCTION

Due to their unconventional magnetic and electronic properties, Ruddlesden-Popper (RP) ruthenates $(Sr, Ca)_{n+1}Ru_nO_{3n+1}$ are attracting increasing interest in the field of solid-state physics and materials science [1]. Notably, $Ca_3Ru_2O_7$ is one of the few known polar metals (which are able to retain a spontaneous electric polarization in the metallic state) [2]. In its $Bb2_1m$ crystalline form [3], $Ca_3Ru_2O_7$ exhibits a rich variety of physical phenomena, including temperature-dependent band dispersion [4–6], pressure-induced magnetic phase transition [3], colossal magnetoresistance [7], strong correlation, and pronounced spin-orbit coupling, making it a prototypical system to study the effects of temperature on the electronic, magnetic, and transport properties of polar metals. Cooled down below its Néel temperature of 56 K, $Ca_3Ru_2O_7$ becomes antiferromagnetic with spins aligned along its a axis (AFM-a). When further cooled down to 48 K, it undergoes a second magnetic phase transition, where spins reorient along the b axis (AFM-b); this transition is accompanied by an isostructural phase transformation (corresponding to a contraction of the unit cell along its c axis) and by a sudden change in resistivity of semimetallic character (often interpreted as arising from the opening of a pseudogap) [5,6,8]. Below 30 K, $Ca_3Ru_2O_7$ undergoes another phase transition whereby it recovers its metallic temperature-dependent resistivity.

While first-principles calculations based on density functional theory (DFT) [9,10] have demonstrated their accuracy in predicting lattice vibrations, electron excitations, and configuration effects [11–14], it is still an ongoing challenge to evaluate the transport properties of materials. For instance, the calculations of electrical conductivities typically rely on the Boltzmann transport theory [15,16] which further needs the electron relaxation times whose values are generally on the order of 10^{-14} s [24]. While the relaxation times can in principle be predicted based on electron-electron scattering [5,17–19], or using the Bardeen-Shockley deformation-potential theory [20,21] under the effective mass approximation together with phenomenological parameters [22,23], the majority of DFT-based calculations [15,19,24] treat them as the scaling parameters.

This work reports the thermal and electrical properties of $Ca_3Ru_2O_7$ from first-principles calculations based on density-functional theory. In this work, first-principles quasiharmonic phonon calculations are carried out to understand the thermodynamic and electrical properties of $Ca_3Ru_2O_7$. A tractable model is proposed to estimate the temperature dependence of the electron relaxation time by correlating electron-relaxation times to the specific heat per mobile charge, as initially suggested by the previous work [25,26].

II. BOLTZMANN TRANSPORT THEORY

The electrical conductivity in the Boltzmann transport theory is written as

$$\boldsymbol{\sigma} = \frac{e^2}{V k_B T} \int_{-\infty}^{\infty} f(1-f)\, \boldsymbol{\Xi}(\varepsilon) d\varepsilon, \tag{1}$$

where e is the elementary charge, V is the volume, T is the temperature, ε is the one-electron energy, and $\boldsymbol{\Xi}(\varepsilon)$ is the so-called the transport function [15,16]. $\boldsymbol{\Xi}(\varepsilon)$ is a tensor with

*yuw3@psu.edu
†yyx5048@psu.edu

components

$$\Xi^{\alpha\beta}(\varepsilon) = \int \sum_i \tau_{i,\boldsymbol{k}} v_i^{\alpha}(\boldsymbol{k}) v_i^{\beta}(\boldsymbol{k}) \delta[\varepsilon - \varepsilon_i(\boldsymbol{k})] \frac{d\boldsymbol{k}}{8\pi^3}, \quad (2)$$

where α and β are the indices labeling the Cartesian axis, i is the one-electron band index, $\tau_{i,\boldsymbol{k}}$ is electron relaxation time, and the electron group velocity v_i^{α} is the gradient of electron band energy with respect to $\boldsymbol{k}$, namely

$$v_i^{\alpha}(\boldsymbol{k}) = \frac{1}{\hbar} \frac{\partial \varepsilon_i(\boldsymbol{k})}{\partial k^{\boldsymbol{\alpha}}} \quad (3)$$

III. A MODEL TO ESTIMATE THE ELECTRON RELAXATION TIME BASED ON HEISENBERG UNCERTAINTY PRINCIPLE

In this section, an attempt is made to propose a tentative model for estimating the electron relaxation time and its temperature dependence based on the outputs from DFT calculations. The initial schematic idea stems from (a) the Heisenberg uncertainty principle as given in Eq. (4) below, and (b) the common belief that the thermal energy per mobile charge carrier is on the scale of k_BT. One may then guess that the electron relaxation time might be roughly on the scale of $\hbar/(2k_BT)$**.** Following this thought, at 300 K, one can obtain a relaxation time of 1.27 $\times 10^{-14}$ s which is very close to the commonly assumed value of 1.0 $\times 10^{-14}$ s for the electron relaxation time in the literature [15,16,24].

Next, we will formulate a procedure to calculate the electron relaxation time. We will follow the constant electron relaxation time approximation, i.e., treat $\tau_{i,\boldsymbol{k}} = \tau$ in Eq. (2). The inspiration is from the Heisenberg uncertainty principle which imposes the lower limit for the product between the measurable uncertainty of energy and the measurable uncertainty of time by

$$\langle \Delta\varepsilon \rangle \langle \Delta t \rangle \geqslant \frac{\hbar}{2}. \quad (4)$$

We propose that the electron relaxation time can be thought of as a kind of time fluctuation for an electron transition from one state to another state. We therefore assume the electron relaxation time is proportional to the measurable uncertainty of time, i.e., $\tau \propto x\langle \Delta t \rangle$, so that we have

$$\langle \Delta\varepsilon \rangle \tau = x\frac{\hbar}{2}, \quad (5)$$

where x can be treated as a material constant, and we found that $x = 0.5$ is a good choice for the present example of $Ca_3Ru_2O_7$ and the FeNbSb half-Heusler (R. Wan, personal communication on using the open source code [27] which was developed based on the present work and forked from BoltzTrap2 [28]).

Continually, we will formulate a procedure to calculate the energy uncertainty $\langle \Delta\varepsilon \rangle$. For the electron system, we assume that the energy uncertainty $\langle \Delta\varepsilon \rangle$ is related to the energy fluctuations $\langle \Delta\varepsilon \rangle^2$ as heat is randomly exchanged between the system and heat bath, i.e.,

$$\langle \Delta\varepsilon \rangle^2 = \langle (\varepsilon - \langle \varepsilon \rangle)^2 \rangle. \quad (6)$$

Furthermore, one knows that $\langle \Delta\varepsilon \rangle^2$ is related to the heat capacity of a particle c by

$$c = \frac{\langle (\varepsilon - \langle \varepsilon \rangle)^2 \rangle}{k_BT^2} \cong \frac{\langle \Delta\varepsilon \rangle^2}{k_BT^2}. \quad (7)$$

For the present case, c will be the heat capacity per mobile charge carriers as rationalized in the previous work [25,26,29],

$$c = \frac{c_{\text{el}}}{n} = \frac{\langle (\varepsilon - \langle \varepsilon \rangle)^2 \rangle}{k_BT^2} \cong \frac{\langle \Delta\varepsilon \rangle^2}{k_BT^2}, \quad (8)$$

where c_{el} is the electronic contribution to the specific heat, and

$$n = \int_{-\infty}^{\infty} (1 - f) f D(\varepsilon) d\varepsilon, \quad (9)$$

where f is the familiar Fermi distribution [30–32] and $D(\varepsilon)$ is the electronic density of states given by

$$D(\varepsilon) = \int \sum_i \delta[\varepsilon - \varepsilon_i(\boldsymbol{k})] \frac{d\boldsymbol{k}}{8\pi^3}. \quad (10)$$

n in Eq. (9) can be considered as the number of the mobile charge carriers, or the number of active electronic thermal carriers. Equation (9) shows that the electronic states near the Fermi level $[\mu(T)]$ [33,34] contributes the most to the electric or thermal conduction as it is dictated by the factor of $(1-f)f$ which mimics an interaction between electron and hole states through f and $(1-f)$, respectively. In other words, the electron system can be viewed as a system made up of mobile charge carriers which makes the main contributions to the electronic heat conductivity, electronic heat capacity, and electric conductivity.

$\langle \varepsilon \rangle$ in Eq. (7) is the average band energy per mobile charge carrier defined as

$$\langle \varepsilon \rangle = \frac{1}{n} \int_{-\infty}^{\infty} \varepsilon (1 - f) f D(\varepsilon) d\varepsilon. \quad (11)$$

c_{el} in Eq. (7) can be calculated by

$$c_{\text{el}} = \frac{1}{k_BT^2} \int_{-\infty}^{\infty} (\varepsilon - \langle \varepsilon \rangle)^2 (1 - f) f D(\varepsilon) d\varepsilon. \quad (12)$$

Finally, substituting Eq. (7) into Eq. (5), one gets

$$\tau = x\frac{\hbar}{2T}\sqrt{\frac{n}{k_Bc_{\text{el}}}}. \quad (13)$$

Note that n and c_{el} can be calculated using Eqs. (9) and (12), respectively.

IV. COMPUTATIONAL DETAILS

A. Electronic-structure calculations

DFT calculations are performed using the Vienna Ab-initio Simulation Package (VASP) with considering spin-orbit interactions. The projected augmented wave method [35,36] LDA [37] (local density approximation) functional is utilized to assess the electron and phonon properties. To account for the strong correlation among the d electrons in Ru, the on-site Coulomb repulsion of 1.2 eV is applied on the 4d orbitals using Dudarev's approach [38]. The initial lattice parameters are taken from experimental measurements [1] at 8 and 50 K, respectively, which correspond to the AFM-b and AFM-a

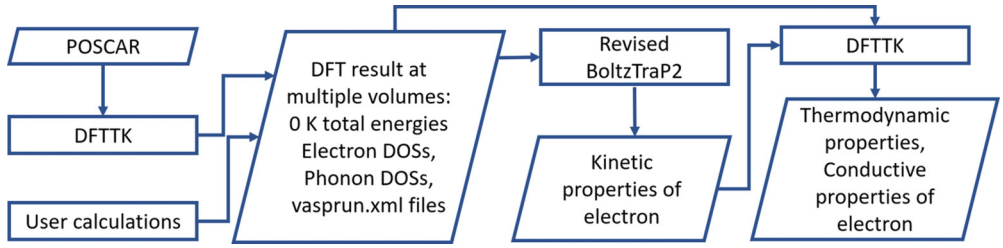

FIG. 1. Computerization of workflow.

magnetic ordering. The optimization of the atomic positions is carried out with a plane-wave cutoff of 650 eV, and the Brillouin zone is sampled using Gaussian smearing with a 20-meV width on a $5 \times 5 \times 3$ Γ-centered k mesh. The energy and forces are converged to be within 10^{-8} eV and 0.1 meV/Å. After the self-consistent calculations, non-self-consistent calculations are performed using denser k mesh of $10 \times 10 \times 6$ for more accurate electronic energy eigenvalues to calculate the transport properties of electrons based on the Boltzmann transport theory [15,16].

B. Computational implementation

The workflow for the computerization is given in Fig. 1. To implement the formulism, we modified the BoltzTrap2 code [28] by adding the functions to calculate the electron heat capacity and effective charge carrier density as described in Eqs. (7) and (9). To make sure of the computational accuracy at the low temperature region, the mesh for the one-electron energy was modified from uniformly sampling to a self-adapted sampling with denser mesh (1000 times) near the Fermi energy by Gaussian distribution. The procedure for calculating the chemical potential of the electron was also revised by implementing Brent's method [39] to improve computational efficiency.

The thermodynamic calculations are performed using the DFFTK package [40] which has been released to the public under the MIT software license. In addition to the routine calculations of thermodynamic properties via the quasiharmonic approach (QHA) [11,41], it has been implemented in DFFTK that any properties, as long as they depend on volume or stain, can be calculated under a quasistatic approach via the predicted property-volume/strain relationship from the QHA [41,42]. Therefore, the effects of thermal expansion have been considered for calculating both the electron relaxation time and the electrical conductivity.

V. RESULTS AND DISCUSSION

A. Heat capacity and Debye temperature

The calculated heat capacities for the AFM-a and AFM-b phases of $Ca_3Ru_2O_7$ are compared with a collection of experimental data [1,43,44] in Fig. 2. They show excellent agreement between the calculations and experiments except for the experimental spike around 48 K. A heat capacity spike in the vicinity of a phase transition temperature is typical for structural phase transitions. The thermal electronic contribution in Eq. (12) is separated from the lattice contribution as

$$C_{p,\mathrm{lat+el}} = c_{\mathrm{el}} + C_{p,\mathrm{lat}}. \tag{14}$$

Figure 2 shows that the electronic contributions are small.

Next, we investigate the behaviors of the heat capacity at the low temperature region as routinely performed [1,44] via the form of C/T vs T^2, namely,

$$C_{p,\mathrm{lat+el}}/T = \gamma + \beta T^2, \tag{15}$$

where γ is the so-called electronic heat capacity coefficient [45], and based on the value of β one can calculate the Debye temperature or vice versa the value of β can be determined once the Debye temperature is known.

Approaching the 0-K limit, we get the Debye temperatures of 492.4 and 476.4 K, for the AFM-b and AFM-a phases, respectively. In comparison, the reported Debye temperature by McCall *et al.* [44] was 480 K based on fitting their measurements. Away from the low temperature region, one can get the Debye temperature by fitting the calculated constant heat capacity from the phonon approach utilizing the Debye formula for the heat capacity [12,46]. Figure 2 shows that the Debye temperatures are moderately temperature dependent.

At the low temperature limit, the calculated γ's by the present work are 0.23 mJ/mol atom and 0.90 mJ/mol atom, for the AFM-b and the AFM-a phases, respectively. In particular, the value of 0.23 mJ/mol atom for the AFM-b phase agrees excellently with the calorimetric result reported by Ke *et al.* [43] and is close to the value of 0.28 mJ/mol atom reported by Yoshida *et al.* [1], whereas it is one magnitude smaller than the value of 3.7 mJ/mol atom as reported by McCall *et al.* [44] and the value of 3.1 mJ/mol atom by Gao *et al.* [47].

B. Calculated physical quantities from the electron density of states

Major thermal properties of electrons can be calculated from the electron density of states [12]. The electron density of states (DOS) calculated for the AFM-b and AFM-a phases are illustrated in Fig. 3(a). At the Fermi energy, the DOS for the AFM-b is roughly half of that of the AFM-a phase. This ratio is quite similar to the measured ratio of the electrical conductivity [5] of the AFM-b to the AFM-a phases. We observed opposite behaviors [5] on the locations of Fermi energies for the two phases, i.e., a dip structure for the AFM-b phase vs a peak structure for the AFM-a phase at the Fermi energy. This observation could correspond to the experimental

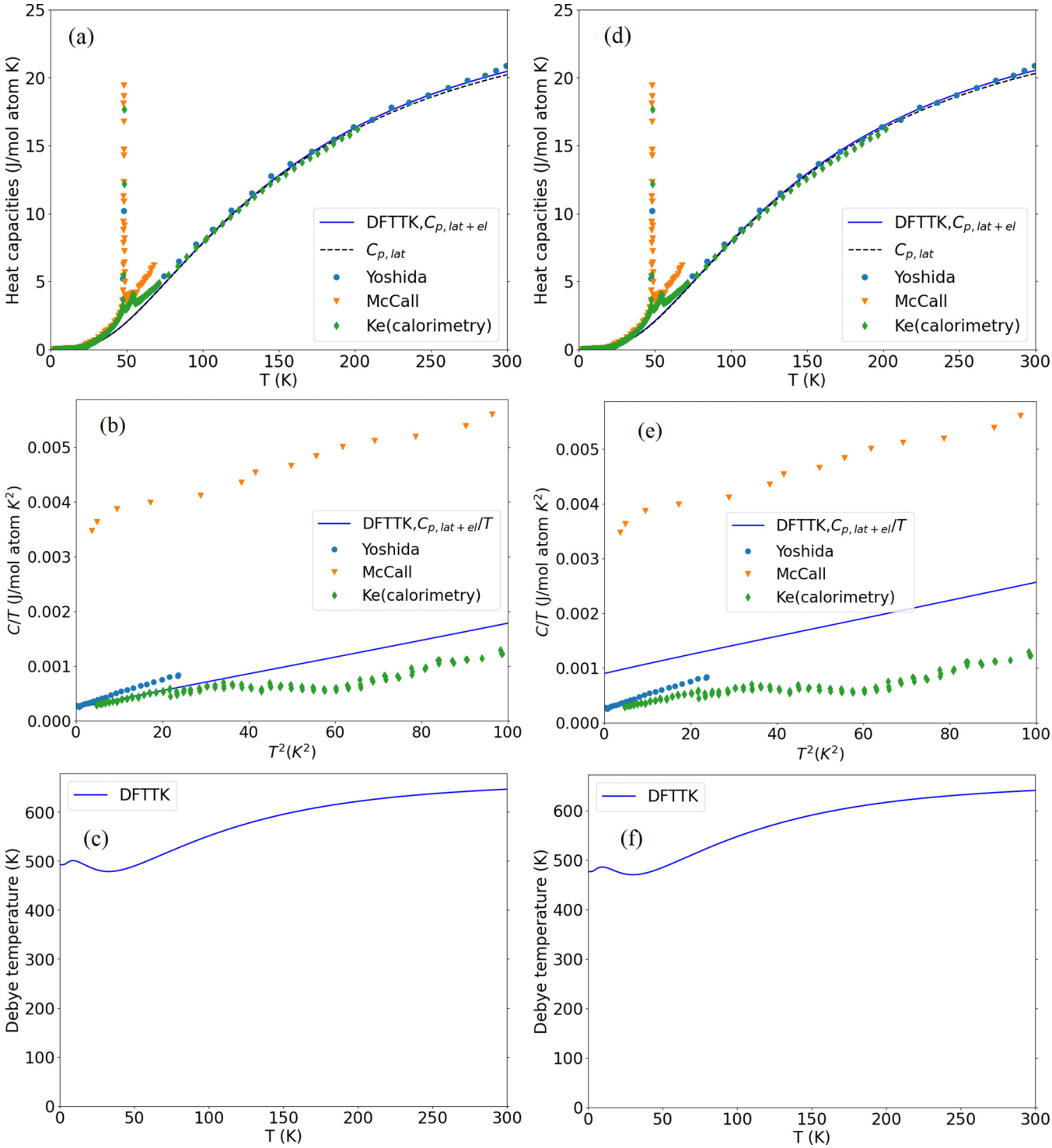

FIG. 2. Heat capacities, electronic heat capacity coefficients, and Debye temperatures for the AFM-*b* [(a), (b), and (c)] and AFM-*a* [(d), (e), and (f)] phases of $Ca_3Ru_2O_7$, respectively. The dots are experimental data [1,43,44]. The dashed lines in the heat capacity plots are for the calculated values without considering the thermal electronic contributions. C/T vs T^2 plot represents the analysis of the heat capacity at low temperature.

suggestion of the appearance of an insulatinglike pseudogap [5].

We hereby want to reiterate the importance of the concept of "mobile charge carriers" as given in Eq. (9) which was introduced in a previous work [25]. On one hand, it showed that only the electronic states with energies around the Fermi level can contribute to the thermal properties, by a factor of $f(1-f)$ to the electron density of states as seen from Eqs. (9), (11), and (12). As a matter of fact, $f(1-f)$ behaves quite like a Dirac delta function except a normalization factor when approaching low temperature. For the two AFM phases of $Ca_3Ru_2O_7$, the calculated mobile charge carriers are

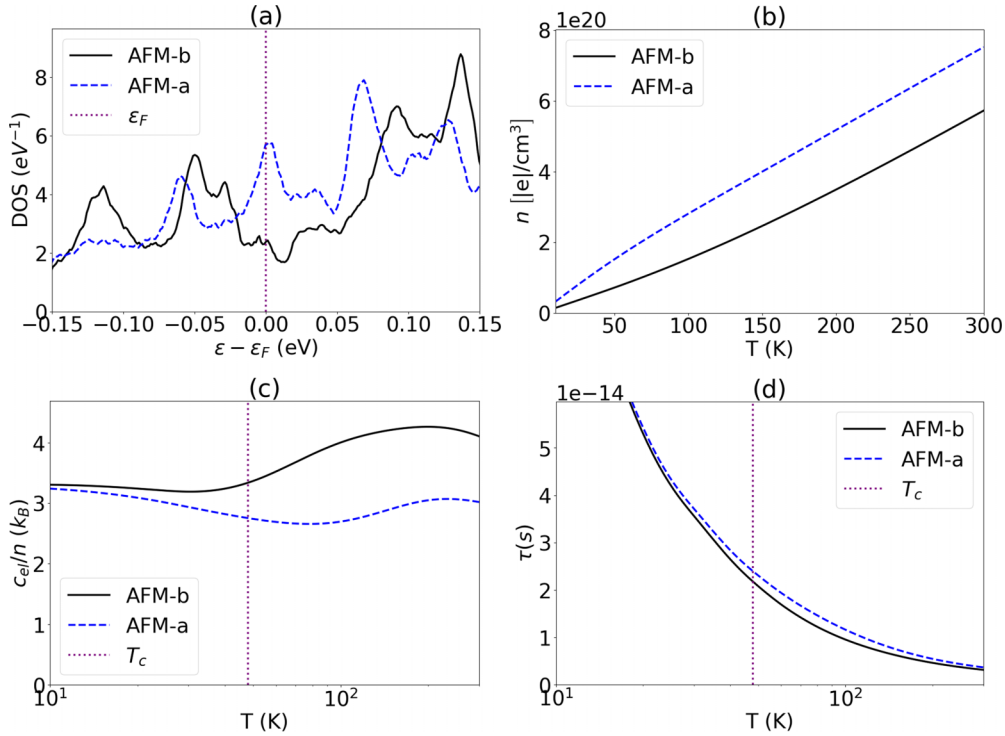

FIG. 3. Calculated electronic properties based on the electron density of states for the AFM-*b* and AFM-*a* phases of $Ca_3Ru_2O_7$. (a) Electron density of states; (b) density of the active electronic thermal carriers; (c) the electronic heat capacity per active electronic thermal carriers; (d) the relaxation time estimated using Eq. (13) based on c_{el}/n in Eq. (7).

illustrated in Fig. 3(b) which shows that the calculated densities of mobile charge carriers for the two phases are nearly linear temperature dependent, typical for metallic materials.

The most important quantity that came into the expression for electron relaxation time in Eq. (13) is the electronic heat capacity per effective mobile charge carriers, namely c_{el}/n in Eq. (7). The calculated c_{el}/n's for the two phases of $Ca_3Ru_2O_7$ are plotted in Fig. 3(c). It shows that the values of c_{el}/n's are roughly constants. This can be understood in terms of the Lorenz number which is a factor of k_B/e^2 to c_{el}/n as we proved in a separate work [26]. Last, plotted in Fig. 3(d) is the estimated electron relaxation time based on Eq. (13) using $x = 0.5$ which is found to be a good fit to match the electrical resistivity measured by Yuan *et al.* [5].

Theoretically, the electron relaxation time was mostly analyzed in terms of the rates of impurity, acoustic phonon, and polar phonon scattering [48,49] as well as electron-electron scattering [5,17–19]. The resulting electron relaxation time (τ) in Eq. (13) could be considered as an effective estimate incorporating all these scatterings in an average way.

In a separate work [26], we proved that c_{el}/n in Eq. (7) is related to the Lorenz number [50,51] by a factor of k_B/e^2. Considering the fact that the Lorenz number was weakly temperature dependent which was especially true for metallic materials [52–55], it was observed from Eq. (13) that the relaxation time by the present work was virtually inversely proportional to the temperature. This temperature proportionality is the same with the recent works, such as Refs. [22,56], which report $\tau = Cn^{-1/3}/T$ where n is the doping level, and C is a fitting parameter. The present temperature proportionality is also the same with Wilson and Block's result for metals [57,58], that obtained from the Umklapp process reported in Ref. [59], and Ziman's results [60,61].

C. Calculated physical quantities from the transport electron density of states

The transport electron density of states is a fundamental quantity to calculate almost all key kinetic properties of electrons [15,16] once the electron relaxation time is known. According to the BoltzTrap2 code [28], the transport electron density of states is defined as

$$\Phi(\varepsilon) = \frac{1}{3}\mathrm{tr}\left[\int \sum_i v_i^{\alpha}(\boldsymbol{k}) v_i^{\beta}(\boldsymbol{k}) \delta[\varepsilon - \varepsilon_i(\boldsymbol{k})] \frac{d\boldsymbol{k}}{8\pi^3}\right], \quad (16)$$

where the mathematical operator tr means to find the trace of a tensor. The calculated transport electron density of states for the two phases of $Ca_3Ru_2O_7$ is illustrated in Fig. 4(a). Compared with the plot of the DOS's given in Fig. 3(a), the pseudogap behavior [5,8] is more evident in the plot of transport electron density of states, i.e., a deep dip structure for the AFM-*b* phase vs a shallow structure for the AFM-*a* phase at the Fermi energy, attributed to the significant differences of the electron group velocities between the two phases.

With the transport electron density of states and the electron relaxation time in hand, we can now investigate the electrical conductive properties and understand the T-dependent gapping [5]. According to the Cutler-Mott theory

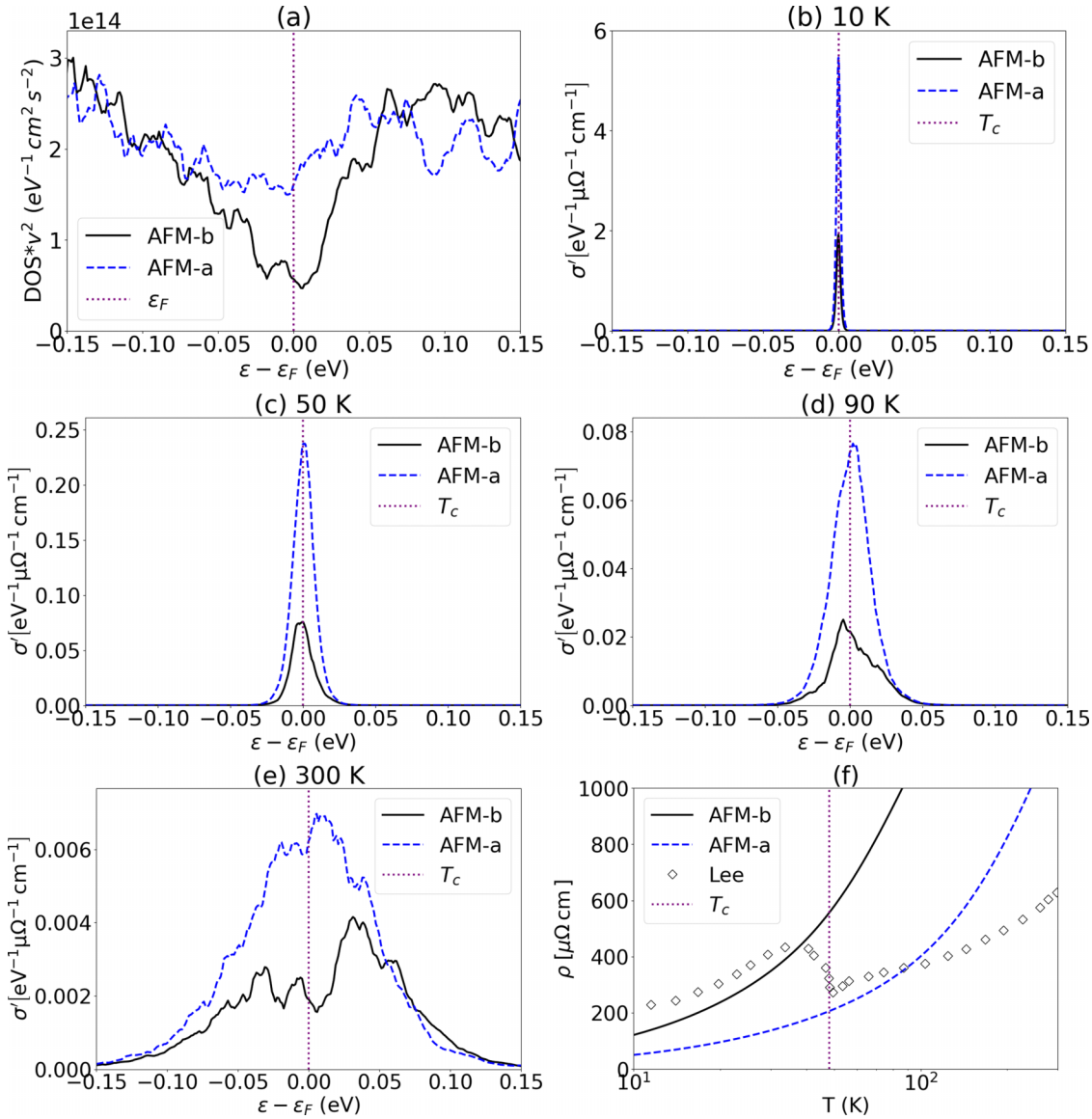

FIG. 4. The calculated conductive properties for the AFM-*b* (solid lines) and AFM-*a* (dashed lines) phases of $Ca_3Ru_2O_7$. (a) Transport density of states of electron as defined in Eq. (16); (b)–(e) Mott energy-dependent differential electrical conductivity at 10, 50, 90, and 300 K, respectively; (f) electrical resistivity. The diamonds in (f) are the experimental dc electrical resistivities reported by Lee *et al.* [8].

[62], the electrical conductivity is formulated as

$$\sigma = \int_{-\infty}^{\infty} \sigma'(\varepsilon) d\varepsilon, \tag{17}$$

where $\sigma'(\varepsilon)$ is a kinetic coefficient called the energy-dependent differential electrical conductivity which is related to the transport density of states in Eq. (16) by

$$\sigma^{'(\varepsilon)} = \frac{e^2}{k_B T V} f(1-f)\Phi(\varepsilon)\tau. \tag{18}$$

Again, it is observed that only the electronic states with energies around the Fermi level can contribute the electrical conductive properties dictated by the factor of $f(1-f)$. In Figs. 4(b)–4(e), we choose $T = 10$, 50, 90, and 300 K to demonstrate the evolutions of the calculated $\sigma'(\varepsilon)$ for the two phases of $Ca_3Ru_2O_7$.

Finally, the calculated electrical resistivities [the inverse of the conductivity given in Eq. (17)] of the AFM-*b* and AFM-*a* phases for $Ca_3Ru_2O_7$ are compared with experiment [8] in Fig. 4(f). Note that a fair comparison with experiment should be only made up to the Néel temperature of 56 K. By experiment [8,43], above 56 K $Ca_3Ru_2O_7$ is paramagnetic which is not handled in the present work.

VI. SUMMARY

First-principles calculations based on density functional theory are carried out for the AFM-*b* and AFM-*a* phases of $Ca_3Ru_2O_7$. For the thermodynamic properties at finite temperature, the lattice vibration was handled by the phonon approach, and the thermal electron excitation was treated by Mermin's finite temperature DFT approach. For the electron transport properties, the Boltzmann transport equation was

solved using the BoltzTraP2 code. The calculated heat capacities agree well with experimental data. Furthermore, a model for estimating the electron relaxation time was proposed so that one can estimate the temperature dependence of the electrical conductivity. The approach has been implemented in the BoltzTraP2 code. Application of the model to the AFM-*b* and AFM-*a* phases of $Ca_3Ru_2O_7$ gives rise to promising results when compared with experiment for the temperature dependencies of the electrical conductivity.

ACKNOWLEDGMENTS

This work was supported by the Computational Materials Sciences Program funded by the U.S. Department of Energy, Office of Science, Basic Energy Sciences, under Award No. DE-SC0020145 (Y.W., Y.X., T.Y., V.G., I.D., and L.-Q.C.). Partial financial support was received from the U.S. department of energy Grant No. DE-SC0023185 (Y.W., S.-L.S., and Z.-K.L.). Y.W. was also partially supported by the Hamer Foundation through the Hamer Professorship. Y.Y. is Sponsored by Shanghai Pujiang Program. Partial support was received from the National Science Foundation (NSF) through Grant No. CMMI-2226976 (Y.W. and Z.-K.L.). First-principles calculations were carried out partially on the LION clusters at Pennsylvania State University supported by the Materials Simulation Center and the Research Computing and Cyberinfrastructure unit at Pennsylvania State University, partially on the resources of NERSC supported by the Office of Science of the U.S. Department of Energy under Contract No. DE-AC02-05CH11231, and partially on the resources of Extreme Science and Engineering Discovery Environment (XSEDE) supported by NSF with Grant No. ACI-1053575. This research received funding from Pennsylvania State University's Institute for Computational and Data Sciences through the ICDS Seed Grant Program. We would like to thank Prof. X. Ke for providing his calorimetric heat capacity data.

[1] Y. Yoshida, I. Nagai, S.-I. Ikeda, N. Shirakawa, M. Kosaka, and N. Môri, Quasi-two-dimensional metallic ground state of $Ca_3Ru_2O_7$, Phys. Rev. B **69**, 220411(R) (2004).

[2] W. X. Zhou and A. Ariando, Review on ferroelectric/polar metals, Jpn. J. Appl. Phys. **59**, SI0802 (2020).

[3] Y. Yoshida, S. I. Ikeda, N. Shirakawa, M. Hedo, and Y. Uwatoko, Magnetic properties of $Ca_3Ru_2O_7$ under uniaxial pressures, J. Phys. Soc. Jpn. **77**, 093702 (2008).

[4] I. Marković *et al.*, Electronically driven spin-reorientation transition of the correlated polar metal $Ca_3Ru_2O_7$, Proc. Natl. Acad. Sci. USA **117**, 15524 (2020)].

[5] Y. Yuan, P. Kissin, D. Puggioni, K. Cremin, S. Lei, Y. Wang, Z. Mao, J. M. Rondinelli, R. D. Averitt, and V. Gopalan, Ultrafast quasiparticle dynamics in the correlated semimetal $Ca_3Ru_2O_7$, Phys. Rev. B **99**, 155111 (2019).

[6] D. Puggioni, M. Horio, J. Chang, and J. M. Rondinelli, Cooperative interactions govern the fermiology of the polar metal $Ca_3Ru_2O_7$, Phys. Rev. Res. **2**, 023141 (2020).

[7] X. N. Lin, Z. X. Zhou, V. Durairaj, P. Schlottmann, and G. Cao, Colossal Magnetoresistance by Avoiding a Ferromagnetic State in the Mott System $Ca_3Ru_2O_7$, Phys. Rev. Lett. **95**, 017203 (2005).

[8] J. S. Lee, S. J. Moon, B. J. Yang, J. Yu, U. Schade, Y. Yoshida, S. I. Ikeda, and T. W. Noh, Pseudogap Dependence of the Optical Conductivity Spectra of $Ca_3Ru_2O_7$: A Possible Contribution of the Orbital Flip Excitation, Phys. Rev. Lett. **98**, 097403 (2007).

[9] P. Hohenberg and W. Kohn, Inhomogeneous electron gas, Phys. Rev. **136**, B864 (1964).

[10] W. Kohn and L. J. Sham, Self-consistent equations including exchange and correlation effects, Phys. Rev. **140**, A1133 (1965).

[11] Y. Wang, Z.-K. Liu, and L.-Q. Chen, Thermodynamic properties of Al, Ni, NiAl, and Ni3Al from first-principles calculations, Acta Mater. **52**, 2665 (2004).

[12] Z. K. Liu and Y. Wang, *Computational Thermodynamics of Materials* (Cambridge University Press, Cambridge, UK, 2016).

[13] Y. Wang, L.-Q. Chen, and Z.-K. Liu, YPHON: A package for calculating phonons of polar materials, Comput. Phys. Commun. **185**, 2950 (2014).

[14] Y. Wang, S. L. Shang, H. Zhang, L. Q. Chen, and Z. K. Liu, Thermodynamic fluctuations in magnetic states: Fe_3Pt as a prototype, Philos. Mag. Lett. **90**, 851 (2010).

[15] T. J. Scheidemantel, C. Ambrosch-Draxl, T. Thonhauser, J. V. Badding, and J. O. Sofo, Transport coefficients from first-principles calculations, Phys. Rev. B **68**, 125210 (2003).

[16] G. D. Mahan and J. O. Sofo, The best thermoelectric, Proc. Natl. Acad. Sci. USA **93**, 7436 (1996).

[17] S. Poncé, E. R. Margine, and F. Giustino, Towards predictive many-body calculations of phonon-limited carrier mobilities in semiconductors, Phys. Rev. B **97**, 121201(R) (2018).

[18] Z. Lin, L. V. Zhigilei, and V. Celli, Electron-phonon coupling and electron heat capacity of metals under conditions of strong electron-phonon nonequilibrium, Phys. Rev. B **77**, 075133 (2008).

[19] S. Poncé, W. Li, S. Reichardt, and F. Giustino, First-principles calculations of charge carrier mobility and conductivity in bulk semiconductors and two-dimensional materials, Rep. Prog. Phys. **83**, 036501 (2020).

[20] J. Bardeen and W. Shockley, Deformation potentials and mobilities in non-polar crystals, Phys. Rev. **80**, 72 (1950).

[21] A. J. Hong, L. Li, R. He, J. J. Gong, Z. B. Yan, K. F. Wang, J.-M. Liu, and Z. F. Ren, Full-scale computation for all the thermoelectric property parameters of half-Heusler compounds, Sci. Rep. **6**, 22778 (2016).

[22] M. Mukherjee, S. Satsangi, and A. K. Singh, A statistical approach for the rapid prediction of electron relaxation time using elemental representatives, Chem. Mater. **32**, 6507 (2020).

[23] R. Farris, M. B. Maccioni, A. Filippetti, and V. Fiorentini, Theory of thermoelectricity in Mg_3Sb_2 with an energy- and temperature-dependent relaxation time, J. Phys.: Condens. Matter **31**, 065702 (2019).

[24] Y. Katsura *et al.*, Data-driven analysis of electron relaxation times in PbTe-Type thermoelectric materials, Sci. Technol. Adv. Mater. **20**, 511 (2019).

[25] Y. Wang, Y. J. Hu, B. Bocklund, S. L. Shang, B. C. Zhou, Z. K. Liu, and L. Q. Chen, First-principles thermodynamic theory of seebeck coefficients, Phys. Rev. B **98**, 224101 (2018).

[26] Y. Wang, J. P. S. Palma, S.-L. Shang, L.-Q. Chen, and Z.-K. Liu, Lorenz number and electronic thermoelectric figure of merit: Thermodynamics and direct DFT calculations, arXiv:2010.00664.

[27] Y. Wang, *Yi Wang /BoltzTraP2 · GitLab*, https://gitlab.com/yiwang62/BoltzTraP2.

[28] G. K. H. Madsen, J. Carrete, and M. J. Verstraete, BoltzTraP2, a program for interpolating band structures and calculating semi-classical transport coefficients, Comput. Phys. Commun. **231**, 140 (2018).

[29] Y. Wang *et al.*, An alternative approach to predict seebeck coefficients: Application to $La_{3-x}Te_4$, Scr. Mater. **169**, 87 (2019).

[30] M. Palumbo, B. Burton, A. Costa e Silva, B. Fultz, B. Grabowski, G. Grimvall, B. Hallstedt, O. Hellman, B. Lindahl, and A. Schneider, Thermodynamic modelling of crystalline unary phases, Phys. Status Solidi **251**, 14 (2014).

[31] G. Grimvall, *Thermophysical Properties of Materials* (Elsevier, Amsterdam, 1999).

[32] S. Baroni, P. Giannozzi, and E. Isaev, Density-functional perturbation theory for quasi-harmonic calculations, Rev. Mineral. Geochem. **71**, 39 (2010).

[33] N. D. Mermin, Thermal properties of the inhomogeneous electron gas, Phys. Rev. **137**, A1441 (1965).

[34] A. K. McMahan and M. Ross, High-temperature electron-band calculations, Phys. Rev. B **15**, 718 (1977).

[35] G. Kresse and J. Furthmüller, Efficiency of ab-initio total energy calculations for metals and semiconductors using a plane-wave basis set, Comput. Mater. Sci. **6**, 15 (1996).

[36] G. Kresse and D. Joubert, From ultrasoft pseudopotentials to the projector augmented-wave method, Phys. Rev. B **59**, 1758 (1999).

[37] J. P. Perdew and A. Zunger, Self-interaction correction to density-functional approximations for many-electron systems, Phys. Rev. B **23**, 5048 (1981).

[38] S. L. Dudarev, G. A. Botton, S. Y. Savrasov, C. J. Humphreys, and A. P. Sutton, Electron-energy-loss spectra and the structural stability of nickel oxide: An LSDA + U study, Phys. Rev. B **57**, 1505 (1998).

[39] P. Virtanen, R. Gommers, T. E. Oliphant, M. Haberland, T. Reddy, D. Cournapeau, E. Burovski, P. Peterson, W. Weckesser, and J. Bright, SciPy 1.0: Fundamental algorithms for scientific computing in Python, Nat. Methods **17**, 261 (2020).

[40] Y. Wang, M. Liao, B. J. Bocklund, P. Gao, S. L. Shang, H. Kim, A. M. Beese, L. Q. Chen, and Z. K. Liu, DFTTK: Density functional theory ToolKit for high-throughput lattice dynamics calculations, Calphad **75**, 102355 (2021).

[41] S.-L. Shang, Y. Wang, D. Kim, and Z.-K. Liu, First-principles thermodynamics from phonon and debye model: Application to Ni and Ni3Al, Comput. Mater. Sci. **47**, 1040 (2010).

[42] Y. Wang, J. J. Wang, H. Zhang, V. R. Manga, S. L. Shang, L.-Q. Chen, and Z.-K. Liu, A first-principles approach to finite temperature elastic constants, J. Phys.: Condens. Matter **22**, 225404 (2010).

[43] X. Ke, J. Peng, W. Tian, T. Hong, M. Zhu, and Z. Q. Mao, Commensurate-incommensurate magnetic phase transition in the Fe-doped bilayer ruthenate $Ca_3Ru_2O_7$, Phys. Rev. B **89**, 220407(R) (2014).

[44] S. McCall, G. Cao, and J. E. Crow, Impact of magnetic fields on anisotropy in $Ca_3Ru_2O_7$, Phys. Rev. B **67**, 094427 (2003).

[45] C. Kittel, *Introduction to Solid State Physics* (John Wiley & Sons, Inc, 2005).

[46] Y. Wang, R. Ahuja, and B. Johansson, Mean-field potential approach to the quasiharmonic theory of solids, Int. J. Quantum Chem. **96**, 501 (2004).

[47] G. Cao, S. McCall, J. E. Crow, and R. P. Guertin, Observation of a Metallic Antiferromagnetic Phase and Metal to Nonmetal Transition in $Ca_3Ru_2O_7$, Phys. Rev. Lett. **78**, 1751 (1997).

[48] V. Fiorentini, R. Farris, E. Argiolas, and M. B. MacCioni, High thermoelectric figure of merit and thermopower in layered perovskite oxides, Phys. Rev. Mater. **3**, 022401(R) (2019).

[49] B. K. Ridley, Polar-optical-phonon and electron-electron scattering in large-bandgap semiconductors, J. Phys.: Condens. Matter **10**, 6717 (1998).

[50] L. Lorenz, Determination of the degree of heat in absolute measure, Ann. Phys. Chem. **147**, 429 (1872).

[51] P. J. Price, The lorenz number, IBM J. Res. Dev. **1**, 147 (1957).

[52] G. S. Kumar, G. Prasad, and R. O. Pohl, Review experimental determinations of the Lorenz number, J. Mater. Sci. **28**, 4261 (1993).

[53] M. Thesberg, H. Kosina, and N. Neophytou, On the Lorenz number of multiband materials, Phys. Rev. B **95**, 125206 (2017).

[54] H. S. Kim, Z. M. Gibbs, Y. Tang, H. Wang, and G. J. Snyder, Characterization of Lorenz number with seebeck coefficient measurement, APL Mater. **3**, 041506 (2015).

[55] X. Wang, V. Askarpour, J. Maassen, and M. Lundstrom, On the calculation of Lorenz numbers for complex thermoelectric materials, J. Appl. Phys. **123**, 055104 (2018).

[56] K. P. Ong, D. J. Singh, and P. Wu, Analysis of the thermoelectric properties of N-Type ZnO, Phys. Rev. B **83**, 115110 (2011).

[57] A. Bulusu and D. G. Walker, Review of electronic transport models for thermoelectric materials, Superlattices Microstruct. **44**, 1 (2008).

[58] A. H. Wilson, *Theory of Metals* (Cambridge University Press, Cambridge, UK, 1953).

[59] J. Mao, Z. Liu, J. Zhou, H. Zhu, Q. Zhang, G. Chen, and Z. Ren, Advances in thermoelectrics, Adv. Phys. **67**, 69 (2018).

[60] J. Yang, R. Liu, Z. Chen, L. Xi, J. Yang, W. Zhang, and L. Chen, Power factor enhancement in light valence band p-type skutterudites, Appl. Phys. Lett. **101**, 022101 (2012).

[61] J. M. Ziman, *Electrons and Phonons: The Theory of Transport Phenomena in Solids* (Clarendon Press, Oxford, 2001).

[62] M. Cutler and N. F. Mott, Observation of Anderson localization in an electron gas, Phys. Rev. **181**, 1336 (1969).